



Kinetics of the evolution of InAs/GaAs quantum dots to quantum rings: A combined x-ray, atomic force microscopy, and photoluminescence study

Vikas Baranwal and Giorgio Biasiol*
Laboratorio Nazionale TASC INFN-CNR, I-34149 Trieste, Italy

Stefan Heun
NEST, CNR-INFN and Scuola Normale Superiore, I-56127 Pisa, Italy

Andrea Locatelli, Tevfik Onur Menten, and Miguel Niño Orti
Sincrotrone Trieste S.C.p.A., I-34149 Trieste, Italy

Lucia Sorba
*NEST, CNR-INFN and Scuola Normale Superiore, I-56127 Pisa, Italy
 and Laboratorio Nazionale TASC INFN-CNR, I-34149 Trieste, Italy*

(Received 14 July 2009; revised manuscript received 3 September 2009; published 27 October 2009)

We present an experimental study of the evolution of InAs/GaAs quantum dots partially capped with GaAs, as an annealing process transforms them first into quantum rings and later into holes penetrating the whole cap layer. Shape, composition, and optical emission were monitored as a function of annealing time by means of atomic force microscopy, x-ray photoemission microscopy, and photoluminescence, respectively. Our results show a progressive dissolution of the original dot, with the outdiffused material forming a second wetting layer on the planar region surrounding the dot. For the longest annealing time, in a situation close to thermodynamic equilibrium, no residual dot material is left in the holes, and an In-rich layer covers uniformly the surface. Our findings were examined by taking into account the surface chemical potential previously written for Stranski-Krastanov islands partially covered with a cap layer. We show that the energy gain due to the formation of the second wetting layer is the driving force for the shape and composition evolution, but its analytical expression should be modified, with respect to previous formulations, by taking into account the observed material interdiffusion.

DOI: [10.1103/PhysRevB.80.155328](https://doi.org/10.1103/PhysRevB.80.155328)

PACS number(s): 81.07.Ta, 68.35.Dv, 79.60.Jv, 68.37.-d

I. INTRODUCTION

The quantum confinement properties of self-assembled quantum dots (QDs) can be deeply mutated by deposition of a thin layer of the barrier material in appropriate conditions and a subsequent annealing, modifying them into so-called quantum rings (QRs).^{1,2} In fact, the material redistribution taking place during this process creates craterlike nanostructures with a nonsimply connected geometry. Thanks to their unique shape, self-assembled QRs possess different electron confinement properties, and thus optical and transport properties, with respect to QDs. As a result, self-assembled QRs can be viewed as a size bridge between mesoscopic and molecular ring structures, exhibiting, for example, the unique property of trapping magnetic flux and persistent currents, not affected by random scatterers.³⁻⁶ For example, they could find a possible application in the detection of terahertz radiation, which has gained much importance for their potential applications in the areas of security and biomedical imaging.^{7,8} Detectors with detection range of 3–10 THz and being operated at high temperatures are of particular interest. Infrared photodetectors based on QRs have the potential of high response speed, low dark and noise current, and it also exhibits the far infrared wavelength detection ability.⁹⁻¹²

A number of experimental studies were concerned with the formation mechanism of InAs/GaAs QRs.¹³⁻¹⁶ The conventional method for the formation of InAs/GaAs QRs is a

capping and annealing procedure, in which a thin GaAs layer is deposited on top of the InAs QDs followed by 30 s of annealing in As₂ flux.^{1,16} During the annealing of the partially capped QDs, a strong material intermixing and redistribution toward the surrounding wetting layer (WL) region takes place.^{1,16} Despite this standard recipe for growing QRs by molecular beam epitaxy (MBE) has been developed, their formation mechanisms are far from being understood, and only some qualitative models have been proposed;^{13,17} thus questions such as the kinetics of the dot-to-ring transition, and the shape and composition of the nanostructures in the limit of thermodynamic equilibrium are still a matter of debate. For example, the dot-to-ring transition has been attributed either to a dewetting process, which expels In from the QDs,⁷ or a simultaneous strongly temperature dependent Ga-In alloying process.¹⁵

In our previous work, we have successfully studied the composition distribution of individual surface InAs/GaAs QRs by chemical maps of single nanostructures obtained by means of laterally resolved photoelectron spectroscopy.¹⁶ In particular, we found that the composition of QRs is not uniform, being In-rich at the center region, corresponding to the residual dot material imaged in buried rings.^{18,19} Our earlier observations on InAs/GaAs QDs suggest that the dot surface composition is neither pure InAs nor homogeneous In_xGa_{1-x}As, but present an In concentration increasing from the borders to the center of the dots.²⁰

In this work, we present an experimental study of the dot-to-ring evolution in the InAs/GaAs system, as a function of annealing time after deposition of the GaAs cap layer, aimed at understanding the kinetics of the transition, and the configuration at the thermodynamic equilibrium limit. Surface profile changes measured by atomic force microscopy (AFM) are correlated with shifts in photoluminescence (PL) emission. By using x-ray photoemission electron microscopy (XPEEM), we obtain two-dimensional compositional maps of unburied rings, which we directly relate to the surface topography measured *ex situ* by AFM. Our observations are interpreted in terms of surface chemical potential distribution, where the wetting term^{21,22} is reconsidered in view of the measured surface composition maps.

II. EXPERIMENTAL

The samples for this study were grown by MBE on GaAs(100) substrates. QDs were formed by depositing 2 monolayers (ML) of InAs at a substrate temperature of 540 °C in As₂ flux. The substrate temperature was then lowered to 490 °C, followed by 2 nm of GaAs deposition and a subsequent annealing for periods varying from 0 to 360 s at the same temperature. Samples for AFM studies were then immediately cooled down and removed from the system. Additional 40 nm of GaAs layer were overgrown at 490 °C on samples for PL spectroscopy measurements. Selected samples for XPEEM analysis were grown on *n*-doped substrates (with annealing times of 0, 30, and 120 s). A protective As layer was overgrown at a substrate temperature of 50 °C for 2 h with an As₄ flux of 2 × 10⁻⁵ Torr to avoid oxidation of the surface when exposed to air during transfer to the XPEEM system.²⁰

AFM measurements of surface topography were carried out in intermittent mode using a Veeco instrument. The surface morphology and the local chemical composition of the sample surfaces were obtained by low energy electron microscopy (LEEM) and XPEEM, respectively, at the Nanospectroscopy beamline at Elettra, Italy. For these experiments, the As capping layer was thermally removed *in situ* at ~380 °C prior to the measurements. A clear (1 × 3) reconstruction was observed by low energy electron diffraction (LEED) after decapping which is typical for As-stabilized InGaAs in a wide composition range.²³ The morphology of decapped samples was checked by *ex situ* AFM, to rule out possible effects of decapping. No differences were found with respect to the QR samples without capping. XPEEM allows obtaining photoemission spectra with an energy resolution of 0.3 eV and a lateral resolution of down to 25 nm.^{24,25} Ga 3*d* and In 4*d* core level spectra were acquired with a photon energy of 80 eV. Laterally resolved photoemission spectra were reconstructed from a series of XPEEM images acquired as a function of photoelectron energy. At the resulting photoelectron kinetic energies for both core levels (~60 eV), the photoelectron escape depth λ is ~0.5 nm, which makes our experiments very surface sensitive (first few ML). For a quantitative evaluation of the composition, we have fitted all spectra with a procedure explained in detail in Refs. 20 and 26. From these fits the total intensities I_{In}, I_{Ga} of the two core levels were extracted.

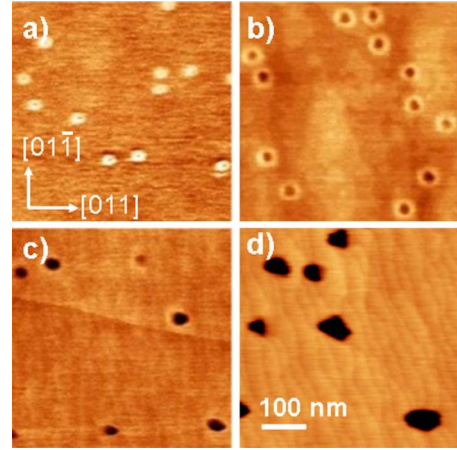


FIG. 1. (Color online) 500 × 500 nm² AFM images of InAs/GaAs QDs capped with 2-nm GaAs followed by (a) 0, (b) 30, (c) 120, and (d) 360 s annealing.

The apparent surface In concentration \bar{x} is given by the relative integrated intensity of the In 4*d* core level to the total intensity, normalized to the respective photoionization cross sections σ (due to the closeness in energy, one can safely assume the same escape depth for both core levels)²⁷

$$\bar{x} = \frac{I_{In}\sigma_{Ga}}{I_{In}\sigma_{Ga} + I_{Ga}\sigma_{In}}. \tag{1}$$

The measured composition, \bar{x} , is a weighted average of the compositions of the topmost atomic layers given as,

$$\bar{x} = \frac{\sum_{i=0}^{\infty} x_i e^{-d_i/\lambda}}{\sum_{i=0}^{\infty} e^{-d_i/\lambda}}, \tag{2}$$

where the contribution of the layer *i* with composition *x_i* at the depth *d_i* is exponentially attenuated with λ. Details of the experimental setup and the analysis can be found in Refs. 20 and 26.

The PL spectra were obtained using an Ar ion laser operated at λ=514.5 nm, corresponding to a photon energy of 2.41 eV, well above the GaAs and InAs energy band gaps. The laser beam is guided and focused through a lens onto the sample. The sample was placed in a closed cycle liquid helium cryostat for low temperature measurements. The luminescence signal dispersed by a 0.5-m monochromator was detected by a Ge photodiode employing standard lock-in technique, and the signal was transmitted to a computer. The measurements were done at 10 K, with an excitation power of 0.5 mW (~6 W/cm²).

III. RESULTS

Figure 1 shows four AFM images for samples with (a) 0, (b) 30, (c) 120, and (d) 360 s annealing time. With increasing annealing, one can notice an overall increase in the nanostructure lateral size, and the development of a central depression, which becomes the only visible feature for the longest annealing times [Figs. 1(c) and 1(d)]. The shape evolution has been evaluated quantitatively in Fig. 2. Figure 2(a)

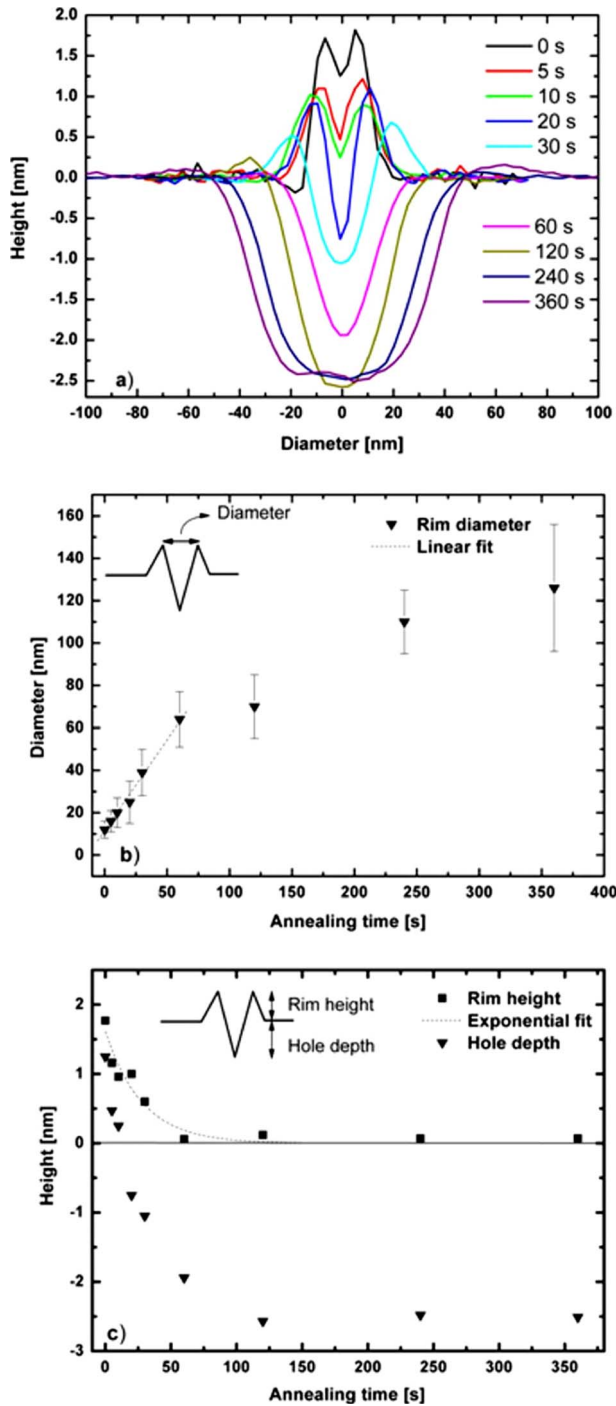


FIG. 2. (Color online) (a) AFM line profiles in the $[01\bar{1}]$ direction for annealing times from 0 to 360 s. (b) Variation in the rim diameter measured at the apex of the rings with annealing time. A linear fit is shown with a dashed line. (c) Variation in the height of the rims and the hole depth with respect to the surrounding planar region as a function of annealing time. The sketches in the insets show the measured quantities.

shows line profiles in the $[01\bar{1}]$ direction for all the annealing times from 0 to 360 s, with very similar profiles in the perpendicular direction $[011]$ (not shown here). Each profile is an average of 10 AFM line scans through the centers of QRs. With no annealing, a substantial height reduction in the origi-

nal QD (see Ref. 20) is observed (from about 15 to about 1.5 nm, above the free surface of the capping layer, i.e., about 3.5 nm by considering also the buried part) with just a very shallow depression in the center, while the lateral size is the same as the QD (~ 25 nm). As the annealing proceeds, the central hole and lateral rims develop, and the overall structure becomes broader and shallower. After 30 s annealing the usual QR shape is achieved, with a central hole about 1.0-nm deep with respect to the surface level. However, for the longest annealing times performed (from 120 s), material redistribution washes out completely the ring structure, leaving only a ~ 2.5 nm deep hole surrounded by a flat region with virtually no rims. The hole depth roughly corresponds to the total thickness of the deposited material [i.e., 2 ML (~ 0.5 nm) InAs+2 nm GaAs], thus the hole extends approximately down to the underlying GaAs substrate. Such structures are very similar to those obtained by capping InAs QDs with a few nm GaAs by metalorganic chemical vapor deposition, where surface kinetics is much faster, and profiles much closer to thermodynamic equilibrium are obtained.²⁸ Fig. 2(b) shows the variation in the diameter of the rims (measured on the rim apex) as a function of annealing time (note that for the longest times the rims are invisible in the AFM images, and barely distinguishable in the averaged profiles of Fig. 2(a), but still allowing for a diameter determination, although with a larger error). Figure 2(c) shows the dependence of the height of the external rims and the depth of the central hole on annealing time, both with respect to the surrounding planar region. The geometry of the measured quantities is shown in the insets of Figs. 2(b) and 2(c). An exponential trend is fitted to the external rim height, according to the discussion presented in Sec. IV. Since after 120 s annealing the hole reaches the GaAs substrate and the shape is preserved (with only a much slower enlargement, as compared to the first stages of evolution), it is likely that a situation close to thermodynamic equilibrium has been substantially reached.

Figures 3(a)–3(c) show LEEM images of a 500×500 nm² area measured after the decapping process for 0, 30, and 120 s annealed samples, respectively. The nanostructures are clearly visible as dark features. For the 30 s annealed sample, the QRs are visible as dark, nearly symmetric, and doughnut-shaped regions.¹⁶ Figs. 3(d)–3(f) show XPEEM images from the same surface regions measured at kinetic energies corresponding to the In $4d$ core level, with a photon energy of 80 eV. A clear bright contrast can be seen for 0 and 30 s [Figs. 3(d) and 3(e)], with In-rich areas corresponding to the QRs, while no contrast is visible for 120 s [Fig. 3(f)].

To assess the local composition, we have acquired photoelectron spectra of the In $4d$ and Ga $3d$ core levels from the island and the WL, measured at a photon energy of 80 eV. Figures 4(a) and 4(b) show the spectra taken at the center of the island marked with a circle (shown in the insets) and the surrounding WL. The spectra clearly demonstrate that the In $4d$ emission is higher at the center of the island, as compared to the WL. We have fitted all spectra for a quantitative evaluation of the composition with the procedure detailed in Ref. 20. One such fit is shown in Fig. 4(c), for the photoelectron spectrum obtained from the 120 s annealed sample.

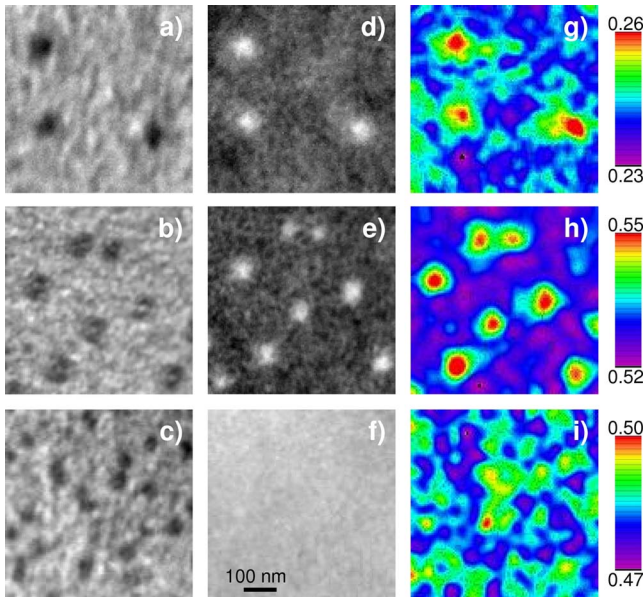


FIG. 3. (Color online) (a–c) $500 \times 500 \text{ nm}^2$ LEEM images of sample surface after decapping for 0, 30, and 120 s annealed samples, respectively. (d–f) XPEEM images from the same surface regions measured at kinetic energies corresponding to the $\text{In } 4d$ core level, with a photon energy of 80 eV. (g–i) Surface In concentration maps of the same regions measured by LEEM and XPEEM. Grayscale images in (a)–(f) are chosen to optimize the contrast, while color scales for images (g)–(i) are indicated at the right.

Maps of the In concentration \bar{x} (obtained with the procedure described in Refs. 20 and 26) of the samples from the same region as for the LEEM images are shown in Figs. 3(g)–3(i). The average In concentration on the planar region was ~ 0.23 , ~ 0.52 , and ~ 0.47 for 0, 30, and 120 s annealed samples, respectively. The substantial drop of surface In concentration from the (uncapped) dot sample ($\bar{x}=0.76$) (Refs. 20 and 26) is mainly caused by the GaAs capping. Outdiffusion of the QD material during GaAs deposition (with a height reduction of about 10 nm of the original dot)²⁰ should not form at this stage a second WL on the planar region, but rather be alloyed with the GaAs cap in the dot surroundings (i.e., on the rims).¹⁷ In fact, the measured composition of the planar region (0.23) agrees well with the one resulting from 2-nm GaAs covering the first WL, with In surface segregation from the WL to the surface.²⁹ For 30 and 120 s annealing, the In surface concentration increases and saturates at about ~ 0.5 (differences between the two samples could result from variations in the deposited In amount and QD density; the lower In concentration for 120 s could also be due in principle to In desorption, but this should not be relevant at 490 °C³⁰). Such extra In presence indicates a strong In redistribution from the original QD to the surface of the surrounding areas during the annealing [Figs. 3(h) and 3(i)]. Thus, despite the fact that the QD material outdiffuses already during GaAs deposition, the second WL is formed only during the subsequent annealing.

Figures 3(g) and 3(h) show that the value of In content, \bar{x} , increases toward the center of the QRs from ~ 0.23 in the WL to ~ 0.26 at the center of the ring for 0 s and from ~ 0.51

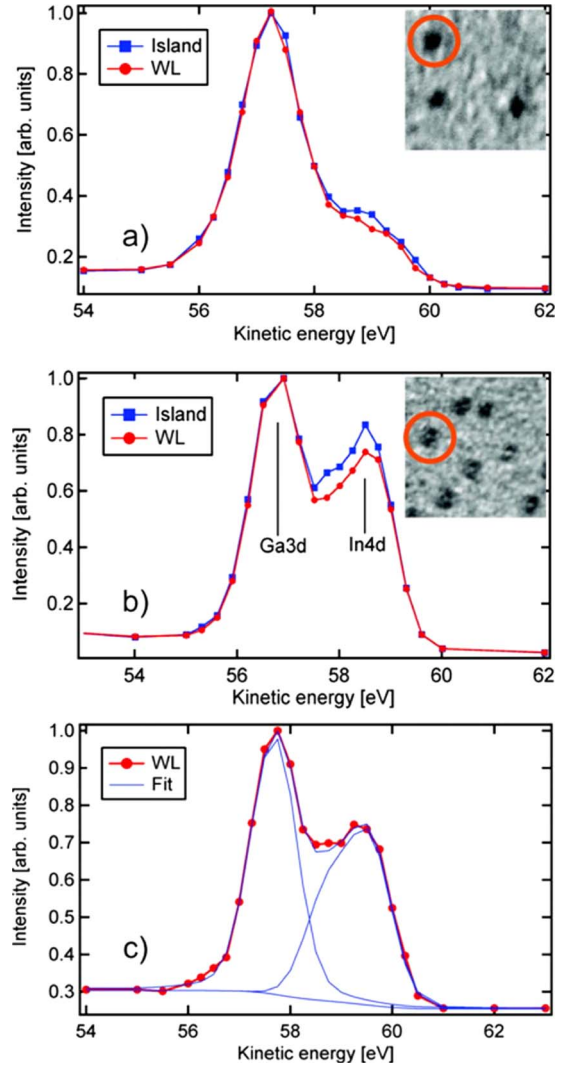


FIG. 4. (Color online) Laterally resolved photoemission spectra of the $\text{In } 4d$ and $\text{Ga } 3d$ core levels from the islands and WL, measured at a photon energy of 80 eV: (a–b) Spectra taken at the center of the island shown in the inset and the surrounding WL for 0 and 30 s annealed samples, respectively. (c) Fit of the spectrum from the WL for the 120 s annealed sample.

to ~ 0.56 for 30 s. On the other hand, for 120 s annealing time, we could not observe any compositional variation [consistent with the $\text{In } 4d$ XPEEM image, Fig. 3(f)] between the QRs and the WL, i.e., a uniform surface composition is observed within our noise level of $\Delta x=0.01$. Thus, as thermodynamic equilibrium is reached, all the QD material is outdiffused resulting in 2.5-nm-deep holes down to the GaAs substrate, and the dot material distributes uniformly on the surface, possibly alloyed with the GaAs capping layer.

To get further insight into the dot-to-ring transition, we have performed PL measurements of the QR emission in GaAs-overgrown samples, for annealing times up to 120 s (i.e., the hole reaches the GaAs substrate). Overgrown structures will likely not be exactly the same as surface QRs, due to segregation or intermixing effects, however, the In-rich core, where optical emission originates, is substantially preserved.¹⁸ The PL emission spectra of the different samples

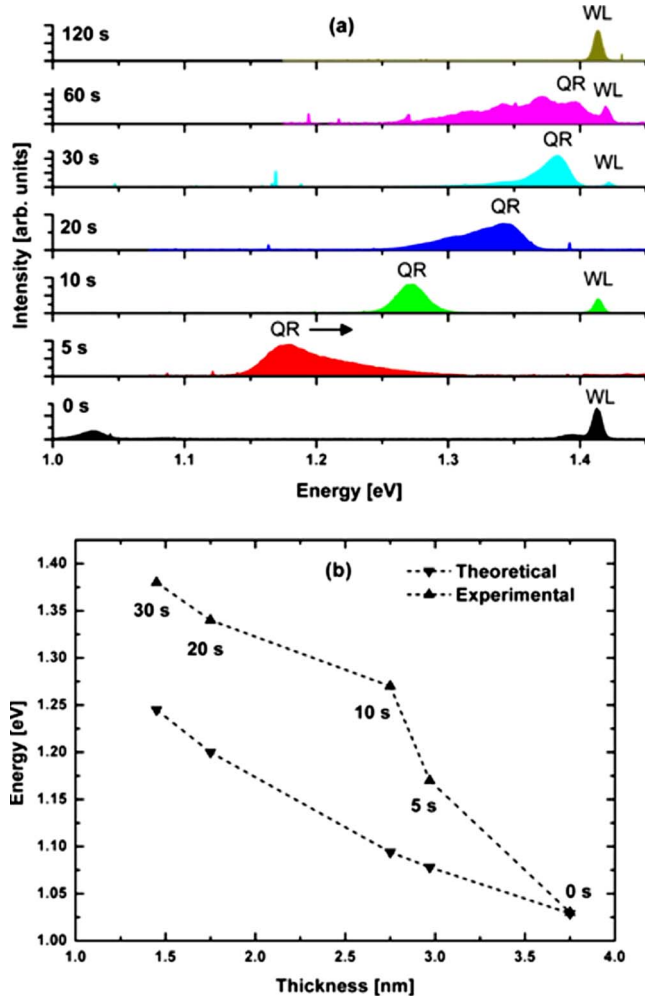


FIG. 5. (Color online) (a) Low temperature PL spectra at 6 W/cm² for samples annealed from 0 to 120 s. A strong blue shift is observed with the increase in annealing time. (b) Evolution of the ground-state emission energy as a function of estimated QR thickness. For details, see text. Triangles: experimental values. Reverse triangles: calculated values assuming a uniform composition $x=0.5$. Annealing times are indicated for each point.

obtained at 10 K are shown in Fig. 5(a). For 0 s annealing, two PL peaks are visible at 1.03 and 1.41 eV, which correspond to QR and WL emission, respectively. Note that at this low power we excited essentially only the ground-state emission, while state filling was observed for higher powers (1.2 mW, not shown). As annealing time increases, the QR emission peak shifts to higher energies.^{2,15,31} The broadness of QR emission for 60 s annealing, with the appearance of multiple peaks, is likely due to the inhomogeneity of the ring thickness at the center, where carriers are confined (see below), that, although similar in the different samples (with a dispersion of about ± 0.3 nm), here becomes comparable to the QR thickness itself (about 0.5 nm). For 120 s annealing, no emission is detected from the QRs, and only a WL peak is visible. This indicates that all the original QD material has diffused away, consistent with the shape and composition profiles. The blue shift in QR emission is systematic with annealing time, similarly to what was observed on InAs/

GaAs QDs subject to partial capping and annealing which transformed them in shallow elongated mounds.³² Such evolution is reasonably due to the increase in the confinement energy as the QR shrinks in height, and to the fact that the residual QD material is more Ga-rich at the base than at the apex.^{20,33} To confirm these conclusions, we have compared our experimental emission energies with calculations on simple model structures (the 60 s sample is not taken into account due to the large uncertainty in its emission energy). Since lateral confinement plays a minor role in determining the ground-state energies,³² we have used a one-dimensional Poisson-Schrödinger solver to estimate them.³⁴ Besides, we assume that carriers are confined essentially in the central core of the QRs, which is justified by the fact that these are the regions richest in Indium.^{18,19} Thus, the QR thickness is obtained by adding or subtracting the hole depth above the free surface [Fig. 2(c)] to the surface-substrate distance (~ 2.5 nm, as explained above). We have then varied the In content in the simulations to match the ground-state energy of the 0 s sample (1.03 eV), which was attained by setting $x \sim 0.5$. This is a reasonable approximation due to In-Ga intermixing, although the actual vertical composition distribution is generally found to be nonuniform. Calculations on the annealed samples by assuming the same composition show that the ground-state emission blue shifts with decreasing thickness, but by amounts that are lower than the observed ones [Fig. 5(b)]. This suggests that the remaining QR material becomes more Ga-rich at its base (thus increasing its band gap), as generally accepted for the original QDs.³³ For example, the ground-state energy of the 30 s sample (1.38 eV) would correspond to $x \sim 0.28$ at the estimated thickness (we have not taken into account possible effects of strain differences). Finally, note that the WL emission does not follow any systematic trend (with only some small sample-to-sample fluctuations), not allowing to follow the formation of the second WL, indicating that a single emission is originating from this planar region with inhomogeneous vertical In distribution.

IV. DISCUSSION

The mechanism of mass transport on an inhomogeneous surface can be related to a gradient of the surface chemical potential μ .³⁵ In the case of self-assembled QDs, μ is modified by the presence of the capping layer, and has been written for In adatoms as,^{21,22}

$$\mu^{\text{In}}(\mathbf{r}) = \mu_0^{\text{In}} + \Omega E_s(\mathbf{r}) + \gamma \Omega \kappa(\mathbf{r}) - \frac{\xi \Omega \vartheta(\mathbf{r})}{a}, \quad (3)$$

where the first term μ_0^{In} is the In chemical potential on a planar unstressed surface, while the second term takes into account the surface elastic energy $E_s(\mathbf{r})$, Ω being the atomic volume. Capillarity (surface shape-related diffusion) is considered in the third term, where γ is the surface energy per unit area and $\kappa(\mathbf{r})$ is the local curvature. The last term formalizes the tendency for In atoms to wet the Ga surface, as a result of the generally lower surface energy of InAs, with respect to GaAs.³⁶ Here ξ is the energy benefit brought by In diffusion on the GaAs cap, a is the lattice parameter, and

$\vartheta(\mathbf{r})$ is 1 on GaAs and 0 on InAs.²¹ At the early stages of overgrowth, incorporation of GaAs above the InAs dots is unfavored because of the large strain relaxation on its surface,^{21,37} thus the first GaAs MLs will not wet the QD. At these stages of growth, therefore, $\vartheta(\mathbf{r})$ was approximated as being 0 on the QD and 1 on the surrounding wetting layer,²² thus determining an outward In flux from the dot. However, as GaAs growth proceeds, the situation is expected to become more complicated. First, after 4 ML, GaAs starts to wet the QD surface,³⁷ possibly alloying with the QD material itself, due to segregation processes;²⁹ second, the outdiffusing In will alloy with the surrounding GaAs. Thus, the difference in surface composition between the QD and the surrounding regions will be reasonably less than almost pure InAs to almost pure GaAs, as assumed for the initial capping,²² with a net decrease in the driving force for In migration.

This is reasonably the situation we obtain after 2-nm GaAs and no annealing [Figs. 1(a), 3(a), 3(d), and 3(g)]: a considerable portion of the original QD has diffused out, leading to a substantial (~ 10 nm) height reduction; however, subsequent wetting of the QD by the GaAs cap has already started. This is confirmed by two observations. First, QDs covered by only 0.5-nm GaAs present a residual height very similar to the 2 nm+0 s annealing case (data not shown here), implying a conformal profile growth beyond 0.5 nm, in agreement with the trend observed in Ref. 37. Second, the apparent In composition on the QDs is reduced to about 0.26, from the original value of 0.85 for uncapped islands;²⁰ with our escape depth, this would be consistent with the presence of a Ga-rich layer above the residual QD material. Thus, the height profile and composition distribution we observe for no annealing suggests that most of the original QD material is outdiffused during deposition of the GaAs cap and strongly alloyed with it, while the cap itself starts to wet the remaining QD. During the subsequent annealing, this remaining In-rich material continues to diffuse, now covering the GaAs cap away from the dots and forming the second WL. This is indicated by the deepening of the central hole and the overall increase in the measured In composition on the surface, as seen above. This process continues until all the QD material has outdiffused, leaving a hole reaching the underlying substrate and a uniform composition. This configuration corresponds to the one predicted by Wang *et al.* at thermal equilibrium, considering the elastic, surface and second WL contribution to the total energy of the system³⁸ (note, however, that in this theoretical work, the energetics of five possible scenarios are examined, which do not include the crater-rim structure of the rings, obtained here as intermediate stages of the dynamical process of QR evolution). The observed trend suggests that the $\vartheta(\mathbf{r})$ factor in the last term of Eq. (3), valid for the early stages of GaAs capping (when In wetting of the cap layer and Ga wetting of the dots are still negligible) could be conveniently substituted by $1-x(r,t)$, which, through the time-varying surface In concentration x (reasonably assumed to be isotropic around each QD) takes into account the local surface composition as the driving force for In wetting. Note that this reduced chemical potential difference is still able to induce outdiffusion of the QD material, as long as a composition gradient is

maintained from the QD to the WL. In fact, our XPEEM experiments show a constant difference of the apparent surface In concentration \bar{x} of about 0.03 up to at least 30 s annealing time [Figs. 3(g) and 3(h)], which goes to zero at 120 s, when the In reservoir of the QDs is exhausted [Fig. 3(i)].

An analytical expression for the profile evolution starting from the chemical potential of Eq. (3) (with the last term modified as suggested above), and using the Nernst-Einstein (NE) and continuity equations,³⁹ would be too difficult to derive, due to the complicated spatial and temporal dependence of the terms in Eq. (3) and to the many (largely unknown) parameters appearing in the same relation. A comparison of our data with Eq. (3), however, allows drawing some general conclusions on the driving forces involved in the diffusion process forming the QRs. First, the existence of a crater as thermodynamic equilibrium is attained [Figs. 1(c) and 1(d)] indicates that the capillarity term (which drives the surface to planarization) should not play a dominant role in the outdiffusion of the original dot material. In fact, Wang *et al.* showed that the surface energy cost upon hole formation is practically balanced by a counteracting elastic energy benefit (due to the removal of the compressively strained, buried part of the QD), and that the total energy change upon the formation of the crater is essentially ascribed to the energy of formation of the second WL.³⁸ Second, Fig. 2(b) shows an initial rapid and constant increase in the rim diameter with time up to 60 s, followed by a much slower expansion at higher times. The NE equation predicts a diffusion flux proportional to the gradient of the surface chemical potential: $J = -(nD/kT)\nabla\mu$, with n the density of adatoms and D the diffusion coefficient. According to Eq. (3), modified as discussed above, the wetting term of $\nabla\mu$ is proportional to the gradient of the surface composition, and by discretizing $\nabla\mu$ into a difference between the QR and WL regions, the NE equation under the effect of wetting can be written as $J \propto \Delta x$, where Δx is the surface composition difference between the two regions. Thus, with a constant Δx , which is maintained until some residual QD material is present, a constant outward flux is expected, as reflected of the linear increase in the rim radius. When the reservoir is exhausted (between 60 and 120 s annealing), Δx drops to zero and wetting-related diffusion stops. The residual, much slower size increase for longer annealing could be due to some residual strain fields in the former dot location, which, however, do not bring about any *qualitative* changes in the nanostructures. Finally, the diameter increase is accompanied by a broadening and a height decrease in the external rims. Contrary to the central hole, capillarity should thus be effective in the thermal smoothening of the rims that, as can be seen in Fig. 2(c), can be well-fitted with an exponential decay, as predicted by Mullins' theory.³⁹

V. CONCLUSION

We have investigated the kinetics of self-assembled QR formation, by monitoring both the shape and composition evolution and the photoluminescence spectra as a function of annealing time. AFM results show that the well-known QR

profile obtained at 30 s annealing time is not a thermodynamic equilibrium profile, but evolves toward a larger hole, reaching the underlying GaAs substrate, with the rim structure completely washed out. Material redistribution mapped by XPEEM shows the formation of a second InAs wetting layer on top of the GaAs cap, distributed uniformly. PL spectra confirm the QD dissolution, resulting in a systematic blue shift in the emission peak with annealing time, until its disappearance (or merging with the WL emission) at 120 s. These results should be taken into account in theoretical models, which so far were able to explain qualitatively only the conventional QR structures formed after 30 s annealing,^{13,22} which are not equilibrium structures. The fact that in samples closer to equilibrium (i. e., for the longest annealing times) the hole reaches the underlying substrate

and the luminescence disappears, indicates that, consistent with thermodynamic calculations,³⁸ virtually all the QD material diffuses out of its original location, merging with the surrounding WL. From a qualitative point of view, by re-examining the surface chemical potential for a partially capped QD at the light of the measured shape and composition evolution, we were able to draw general conclusions on the driving forces involved in the wetting QD dissolution process.

ACKNOWLEDGMENT

We wish to acknowledge the support from the project MIUR-FIRB under Grant No. RBIN06JB4C.

*Corresponding author. biasiol@tasc.infm.it

- ¹J. M. García, G. Medeiros-Ribeiro, K. Schmidt, T. Ngo, J. L. Feng, A. Lorke, J. Kotthaus, and P. M. Petroff, *Appl. Phys. Lett.* **71**, 2014 (1997).
- ²H.-S. Ling and C.-P. Lee, *J. Appl. Phys.* **102**, 024314 (2007).
- ³N. A. J. M. Kleemans *et al.*, *Phys. Rev. Lett.* **99**, 146808 (2007).
- ⁴A. Lorke, R. J. Luyken, A. O. Govorov, J. P. Kotthaus, J. M. García, and P. M. Petroff, *Phys. Rev. Lett.* **84**, 2223 (2000).
- ⁵R. J. Warburton, C. Schaflein, D. Haft, F. Bickel, A. Lorke, K. Karrai, J. M. García, W. Schonefeld, and P. M. Petroff, *Nature (London)* **405**, 926 (2000).
- ⁶V. M. Fomin, V. N. Gladilin, J. T. Devreese, N. A. J. M. Kleemans, and P. M. Koenraad, *Phys. Rev. B* **77**, 205326 (2008).
- ⁷C. Zandonella, *Nature (London)* **424**, 721 (2003).
- ⁸G. L. Carr, M. C. Martin, W. R. McKinney, K. Jordan, G. R. Neil, and G. P. Williams, *Nature (London)* **420**, 153 (2002).
- ⁹E. Räsänen, A. Castro, J. Werschnik, A. Rubio, and E. K. U. Gross, *Phys. Rev. Lett.* **98**, 157404 (2007).
- ¹⁰Y. Xie, W. Chu, and S. Duan, *Appl. Phys. Lett.* **93**, 023104 (2008).
- ¹¹G. Huang, W. Guo, P. Bhattacharya, G. Ariyawansa, and A. G. U. Perera, *Appl. Phys. Lett.* **94**, 101115 (2009).
- ¹²J. H. Dai, J. H. Lee, and S. C. Lee, *IEEE Photon. Technol. Lett.* **20**, 1372 (2008).
- ¹³R. Blossey and A. Lorke, *Phys. Rev. E* **65**, 021603 (2002).
- ¹⁴A. Lorke, R. Blossey, J. M. García, M. Bichler, and G. Abstreiter, *Mater. Sci. Eng., B* **88**, 225 (2002).
- ¹⁵D. Granados and J. M. García, *Appl. Phys. Lett.* **82**, 2401 (2003).
- ¹⁶G. Biasiol, R. Magri, S. Heun, A. Locatelli, T. O. Mentès, and L. Sorba, *J. Cryst. Growth* **311**, 1764 (2009).
- ¹⁷A. Lorke, R. J. Luyken, J. M. García, and P. M. Petroff, *Jpn. J. Appl. Phys.* **40**, 1857 (2001).
- ¹⁸P. Offermans, P. M. Koenraad, J. H. Wolter, D. Granados, J. M. García, V. M. Fomin, V. N. Gladilin, and J. T. Devreese, *Appl. Phys. Lett.* **87**, 131902 (2005).
- ¹⁹D. Granados, J. M. García, T. Ben, and S. I. Molina, *Appl. Phys. Lett.* **86**, 071918 (2005).
- ²⁰G. Biasiol, S. Heun, G. B. Golinelli, A. Locatelli, T. O. Mentès, F. Z. Guo, C. Hofer, C. Teichert, and L. Sorba, *Appl. Phys. Lett.* **87**, 223106 (2005).
- ²¹N. N. Ledentsov *et al.*, *Phys. Rev. B* **54**, 8743 (1996).
- ²²R. Songmuang, S. Kiravittaya, and O. G. Schmidt, *J. Cryst. Growth* **249**, 416 (2003).
- ²³P. A. Bone, J. M. Ripalda, G. R. Bell, and T. S. Jones, *Surf. Sci.* **600**, 973 (2006).
- ²⁴A. Locatelli, A. Bianco, D. Cocco, S. Cherifi, S. Heun, M. Marsi, M. Pasqualetto, and E. Bauer, *J. Phys. IV* **104**, 99 (2003).
- ²⁵T. Schmidt, S. Heun, J. Slezak, J. Diaz, K. C. Ponce, G. Lilienkamp, and E. Bauer, *Surf. Rev. Lett.* **5**, 1287 (1998).
- ²⁶S. Heun, G. Biasiol, V. Grillo, E. Carlino, L. Sorba, G. B. Golinelli, A. Locatelli, T. O. Mentès, and F. Z. Guo, *J. Nanosci. Nanotechnol.* **7**, 1721 (2007).
- ²⁷J. J. Yeh and I. Lindau, *At. Data Nucl. Data Tables* **32**, 1 (1985).
- ²⁸E. Steimetz, T. Wehnert, H. Kirmse, F. Poser, J. T. Zettler, W. Neumann, and W. Richter, *J. Cryst. Growth* **221**, 592 (2000).
- ²⁹O. Dehaese, X. Wallart, and F. Mollot, *Appl. Phys. Lett.* **66**, 52 (1995).
- ³⁰F. Fournier, R. A. Metzger, A. Doolittle, A. S. Brown, C. Carter-Coman, N. M. Jokerst, and R. Bicknell-Tassius, *J. Cryst. Growth* **175-176**, 203 (1997).
- ³¹J. M. García, D. Granados, J. P. Silveira, and F. Briones, *Microelectron. J.* **35**, 7 (2004).
- ³²L. Wang, A. Rastelli, and O. G. Schmidt, *J. Appl. Phys.* **100**, 064313 (2006).
- ³³A. Rosenauer, D. Gerthsen, D. Van Dyck, M. Arzberger, G. Böhm, and G. Abstreiter, *Phys. Rev. B* **64**, 245334 (2001).
- ³⁴<http://www.nd.edu/~gsnider/>
- ³⁵D. J. Srolovitz, *Acta Metall.* **37**, 621 (1989).
- ³⁶L. G. Wang, P. Kratzer, and M. Scheffler, *Jpn. J. Appl. Phys.* **39**, 4298 (2000).
- ³⁷G. Costantini, A. Rastelli, C. Manzano, P. Acosta-Diaz, R. Songmuang, G. Katsaros, O. G. Schmidt, and K. Kern, *Phys. Rev. Lett.* **96**, 226106 (2006).
- ³⁸L. G. Wang, P. Kratzer, M. Scheffler, and Q. K. K. Liu, *Appl. Phys. A: Mater. Sci. Process.* **73**, 161 (2001).
- ³⁹W. W. Mullins, *J. Appl. Phys.* **28**, 333 (1957).